JACS
JOURNAL OF THE AMERICAN CHEMICAL SOCIETY
Communication
pubs.acs.org/JACS

Flexible–Robust Metal–Organic Framework for Efficient Removal of Propyne from Propylene

Libo Li,[†,‡,⊥,#] Rui-Biao Lin,[‡,#] Rajamani Krishna,[§] Xiaoqing Wang,[†,⊥] Bin Li,[‡] Hui Wu,[∥] Jinping Li,[*,†,⊥] Wei Zhou,[*,∥] and Banglin Chen[*,‡]

[†]College of Chemistry and Chemical Engineering, Taiyuan University of Technology, Taiyuan, Shanxi 030024, P. R. China
[‡]Department of Chemistry, University of Texas at San Antonio, One UTSA Circle, San Antonio, Texas 78249-0698, United States
[§]Van't Hoff Institute for Molecular Sciences, University of Amsterdam, Science Park 904, 1098 XH Amsterdam, The Netherlands
[∥]NIST Center for Neutron Research, National Institute of Standards and Technology, Gaithersburg, Maryland 20899-6102, United States
[⊥]Shanxi Key Laboratory of Gas Energy Efficient and Clean Utilization, Taiyuan, Shanxi 030024, P. R. China

Supporting Information

ABSTRACT: The removal of trace amounts of propyne from propylene is critical for the production of polymer-grade propylene. We herein report the first example of metal–organic frameworks of flexible–robust nature for the efficient separation of propyne/propylene mixtures. The strong binding affinity and suitable pore confinement for propyne account for its high uptake capacity and selectivity, as evidenced by neutron powder diffraction studies and density functional theory calculations. The purity of the obtained propylene is over 99.9998%, as demonstrated by experimental breakthrough curves for a 1/99 propyne/propylene mixture.

As novel porous materials, metal–organic frameworks (MOFs) have found various applications in gas storage, separation, sensing, catalysis, and so on because of their unique pore structures and designable frameworks.[1] Research on porous MOFs for gas separation and purification has been mainly focused on those robust MOFs (Scheme 1c).[2] Although

Scheme 1. Schematic Illustration of the Representative Adsorption Isotherms of (a) Flexible, (b) Flexible–Robust, and (c) Robust MOFs

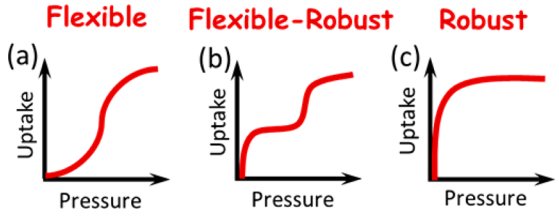

flexible or dynamic MOFs (Scheme 1a) can be theoretically useful as well for gas separation and purification, as indicated by their single gas sorption isotherms, they have rarely been explored for separation of gas mixtures,[3] mainly because the separation performance of flexible MOFs for gas mixtures can be hardly predicted from their single gas sorption isotherms. Once gas molecules of one type open the pore windows/spaces of the flexible MOFs, the opened spaces will simultaneously take up other gas molecules as well.[4] Furthermore, flexible MOFs typically take up negligible amounts of gas at low pressure, making them unsuitable for gas purification, in which trace impurities from gas mixtures need to be efficiently removed.[5]

During our exploration of porous MOFs for gas separation, we realized that one unique class of porous MOFs, so-called flexible–robust ones (Scheme 1b), has basically been overlooked.[6] This class of porous MOFs is different from traditional flexible (Scheme 1a) and robust ones (Scheme 1c) in that their guest-free phases or intermediate phases possess robust pore structures. These phases can preserve their overall structures within a substantial low-pressure range (before the structures become fully flexible and transform into large-pore phases at higher gas pressures) and correspondingly exhibit well-defined plateaus in their multistep adsorption isotherms. Exploration of such flexible–robust MOFs can not only significantly broaden our choices of suitable porous MOFs for gas separation but also provide us the possibility to make use of different robust phases for gas separation (such flexible–robust MOFs will exhibit adsorbate-dependent gas sorption isotherms and thus can be theoretically applied to separations of different types of gas mixtures). In this regard, a previously reported flexible–robust MOF, $[Cu(bpy)_2(OTf)_2]$ (ELM-12) (bpy = 4,4′-bipyridine, OTf^- = trifluoromethanesulfonate),[7] is of special interest. Its flexible–robust nature has been exclusively established through N_2 gas sorption isotherms and the inclusions of different solvent molecules (e.g., methanol and tetrahydrofuran). Herein we report its application for propyne (C_3H_4)/propylene (C_3H_6) separation, in which trace amounts of C_3H_4 can be readily removed from a C_3H_4/C_3H_6 (1/99) mixture to produce high-purity propylene (over 99.9998%) under ambient conditions. As one of most important chemical products (over 120 million tons produced in 2016), propylene is currently produced by steam cracking in petroleum refining. The raw C_3H_6 product contains a trace impurity of C_3H_4, which is highly undesirable.[8] The C_3H_4 concentration in

Received: April 26, 2017
Published: June 5, 2017

DOI: 10.1021/jacs.7b04268
J. Am. Chem. Soc. 2017, 139, 7733–7736

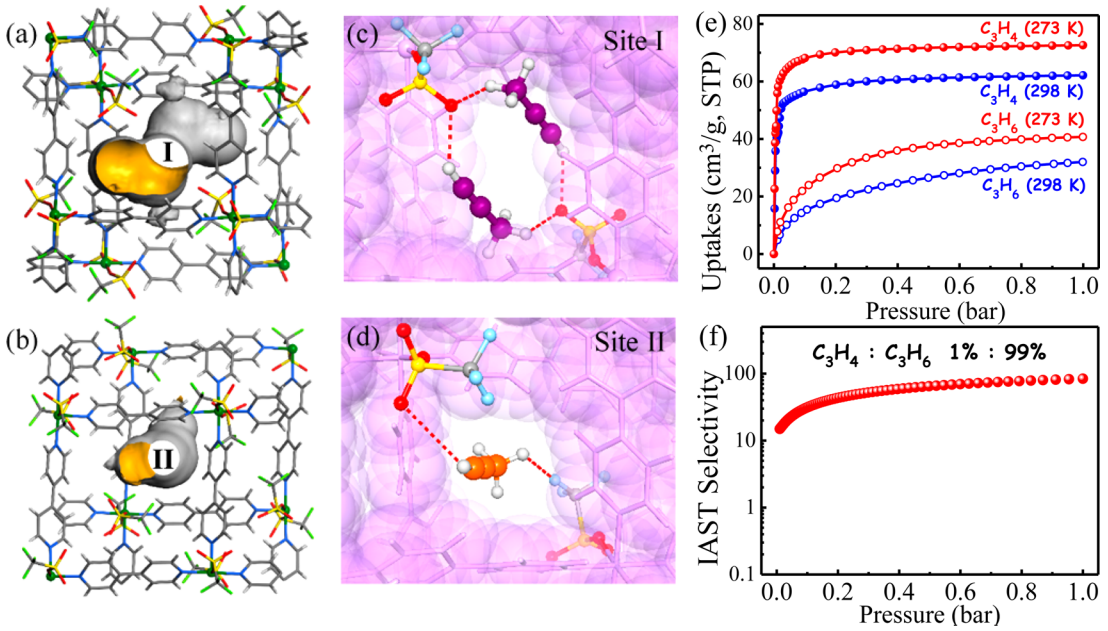

Figure 1. (a, b) Schematic diagrams of the two types of cavities (I and II) in ELM-12 (Cu, green; C, gray; O, red; S, yellow; F, light green). (c, d) Neutron diffraction crystal structure of **ELM-12⊃C_3D_4** showing the preferential binding sites for C_3D_4 molecules (sites I and II) and their close contacts with the framework. (e) C_3H_4 and C_3H_6 adsorption isotherms of ELM-12. (f) Predicted selectivity of ELM-12 for C_3H_4/C_3H_6 (1/99) at 298 K.

polymer-grade propylene is required to be lower than 5 ppm.[8c] Compared with cryogenic distillation and catalytic hydrogenation, adsorptive separation using porous materials is more environmentally friendly and energy-efficient. However, their similar molecular sizes (kinetic diameters: C_3H_4, ~4.76 Å; C_3H_6, ~4.68 Å)[9] make C_3H_6 purification a great challenge.

ELM-12 consists of a rigid square-grid copper bipyridine scaffold with dynamic dangling OTf^- groups. After guest removal, ELM-12 still shows porosity (void fraction = 20.5%, pore volume = 0.141 cm^3/g; see Table S2)[7a] with two kinds of cavities (I and II; see Figure 1a,b). Type I cavities are dumbbell-shaped with small pockets (6.1 Å × 4.3 Å × 4.3 Å) at each end that are connected to each other through a small aperture (3.2 Å × 4.3 Å). Type II cavities are ellipsoid-shaped with a size of 6.8 Å × 4.0 Å × 4.2 Å and are separated from type I cavities by dynamic OTf^- groups. These cavities match well with the size and shape of C_3H_4 (6.2 Å × 3.8 Å × 3.8 Å, compared with 6.5 Å × 4.0 Å × 3.8 Å for C_3H_6), suggesting a potential application for C_3H_4 separation.

Single-component adsorption isotherms of guest-free ELM-12 for C_3H_4 and C_3H_6 were measured at 273 and 298 K (Figure 1e). The C_3H_4 sorption isotherm of ELM-12 exhibits type I character with a sharp increase at low pressure (≤0.01 bar), and the uptake reaches 1.83 mmol/g (41 cm^3/g) at 298 K and 0.01 bar (2.37 mmol/g, 53 cm^3/g at 273 K and 0.01 bar). The corresponding isosteric heat of adsorption (Q_{st}) was calculated to be 60.6 kJ/mol at zero coverage (Figure S2), which is slightly higher than Q_{st} for C_2H_2 discovered in other MOFs with specific binding sites.[2a] The high capacity and relatively strong binding affinity of ELM-12 for C_3H_4 at low pressure indicate that it could be a promising material for the capture of C_3H_4 as a trace component in C_3H_4/C_3H_6 mixtures. Furthermore, the C_3H_4 adsorption capacity of ELM-12 increases to 2.55 mmol/g at 0.1 bar, about 93% of the total uptake at 298 K and 1.0 bar, which is critical for C_3H_6 purification. In contrast, the C_3H_6 adsorption capacity of ELM-12 is relatively low (0.67 mmol/g at 0.1 bar and 298 K) with a far smaller Q_{st} of 15.8 kJ/mol, which implies much weaker host−guest interaction compared with C_3H_4. These results suggest that high C_3H_4/C_3H_6 selectivity of ELM-12 for C_3H_6 purification is quite likely, breaking the stereotype that flexible porous materials are inferior for gas separation.

Next, to predict the adsorption selectivity of C_3H_4/C_3H_6 mixtures, ideal adsorbed solution theory (IAST) calculations were performed on both 1/99 and 50/50 C_3H_4/C_3H_6 mixtures at 298 K (Figures 1f and S3). As expected, ELM-12 exhibits very high C_3H_4/C_3H_6 selectivities, up to 84 for the 1/99 mixture and 279 for the 50/50 mixture, and its C_3H_4 uptake from the C_3H_4/C_3H_6 (1/99) mixture is 0.881 mmol/g (Figures S3 and S4). The calculated exceptional performance of flexible ELM-12 for C_3H_4 adsorption is rare, as indicated by the abnormally high capacity at low pressure, whereas common flexible MOFs typically exhibit negligible gas uptakes under similar conditions.

To determine the nature of C_3H_4 binding in this MOF structure, high-resolution neutron powder diffraction (NPD) measurements were carried out on a C_3D_4-loaded sample of ELM-12 at 298 K (Figures S5 and S6). Two preferential C_3H_4 adsorption sites were clearly identified from the data, as shown in Figure 1c,d. Two C_3D_4 molecules were found to be centrosymmetrically located in cavity I. Each C_3D_4 in cavity I binds to two OTf^- groups (from two different nets) through relatively short C−D···O hydrogen bonds (D···O, 2.31−2.36 Å; C−D···O, 2.80−3.16 Å), which is consistent with the large Q_{st} for C_3H_4 observed in ELM-12. Interestingly, hydrogen-bonding interactions between alkyne and sulfonate groups have also been observed in ionic liquids containing sulfonates.[10] In cavity II, the C_3D_4 molecule shows a weaker binding affinity, as implied by its lower occupancy and longer hydrogen bond (D···O, 3.07 Å). Structure comparison reveals that the dynamic OTf^- adjusts its position/orientation accordingly upon C_3H_4 loading, while the overall crystal lattice stays nearly unchanged

DOI: 10.1021/jacs.7b04268
J. Am. Chem. Soc. 2017, 139, 7733−7736

(the average interlayer distance increases by only ~2%). Also, the geometric pore volume (0.145 cm^3/g) remains almost the same as that of guest-free ELM-12. In comparison, the fully opened ELM-12 has a pore volume of 0.287 cm^3/g, as observed from the N_2-loaded structure (Table S2).[7b] Thus, only the robust intermediate phase of guest-free ELM-12 is utilized for C_3H_4 adsorption under ambient conditions.

To further understand the mechanism of the selective C_3H_4/C_3H_6 adsorption in ELM-12, we conducted detailed first-principles dispersion-corrected density functional theory (DFT-D) calculations. The optimized C_3H_4 binding configurations agree well with the C_3D_4-loaded structure determined from the NPD data. For the two binding sites, the DFT-D-calculated static binding energies (E_B) are ~53.5 and ~45.0 kJ/mol, respectively. In contrast, the binding affinity of C_3H_6 in ELM-12 is significantly lower than that of C_3H_4, with calculated binding energies of only ~32.3 and ~25.6 kJ/mol for the two sites, respectively (Figure S7). All of these results from DFT-D calculations are fully consistent with those from the experimental studies, well supporting that the high C_3H_4/C_3H_6 adsorption selectivity originates from the strong binding of C_3H_4 with the polar OTf^- groups and the confinement of suitable pore geometry in ELM-12 for the sieving effects (Figure S8).

Next, to demonstrate the feasibility of C_3H_4/C_3H_6 separation, transient breakthrough simulations were conducted for ELM-12 in fixed-bed adsorption processes. C_3H_6 first eluted through the bed to yield a polymer-grade gas, and then C_3H_4 broke through from the bed at a long time τ_{break} (Figure S9). These simulation results indicate that ELM-12 can efficiently remove trace C_3H_4 from C_3H_6 gas (1/99 mixture).

In actual breakthrough experiments, 1/99 and 50/50 C_3H_4/C_3H_6 mixtures were used as feeds to mimic the industrial process conditions (Figures 2a and S10). The trace C_3H_4 was efficiently removed from C_3H_6 in the fixed bed to yield a polymer-grade gas. The purity of C_3H_6 monitored at the outlet was >99.9998%, which indicated that the C_3H_4 impurity was completely removed by the ELM-12 material to a concentration below 2 ppm. Furthermore, ELM-12 also exhibited excellent separation performance for the 50/50 C_3H_4/C_3H_6 mixture, reducing the C_3H_4 impurity concentration to <10 ppm. In the practical production process of polymer-grade C_3H_6, the feed gases are also contaminated by trace levels of C_3H_8 (<100 ppm), C_2H_4 (<50 ppm), and CO_2 (<50 ppm). Therefore, a breakthrough experiment with these impurities in the 1/99 C_3H_4/C_3H_4 mixture was also performed for ELM-12 (Figure S11). The results indicate that the presence of C_3H_8, C_2H_4, and CO_2 has nearly no effect on ELM-12 for the separation of C_3H_4 from C_3H_6.

In the normal industrial environment, the adsorbent should also possess good regenerability and structural stability. To ensure the regenerability of ELM-12, C_3H_4 adsorption and 1/99 C_3H_4/C_3H_6 separation cycling experiments were further performed at 298 K (Figures 2b, S12, and S13). The experimental cycling results indicate that there was no noticeable loss in the C_3H_4 adsorption and separation capacity for ELM-12 after 20 cycles. Furthermore, in order to check the structural stability of ELM-12, an aged ELM-12 sample was measured by powder X-ray diffraction (PXRD), IR spectroscopy, C_3H_4 adsorption, and 1/99 C_3H_4/C_3H_6 separation at 298 K (Figure S14). Notably, ELM-12 can retain its structure, uptake capacity, and separation performance after 2 years of storage under ambient conditions.

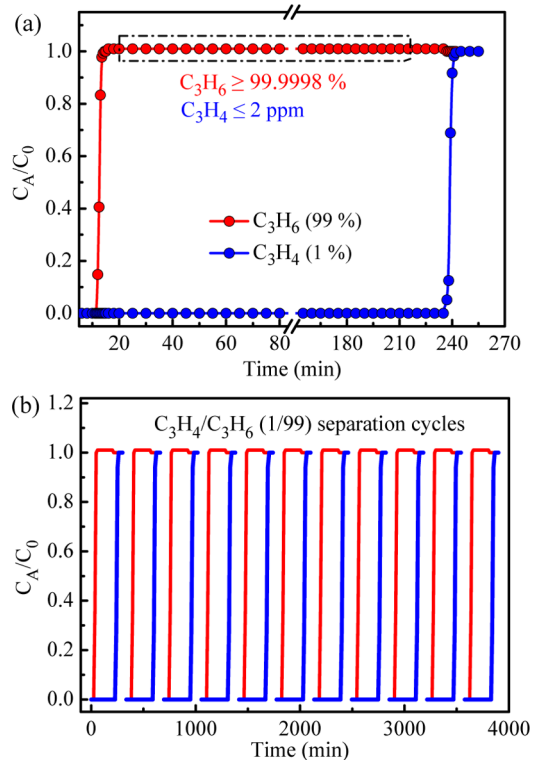

Figure 2. (a) Experimental column breakthrough curves for a C_3H_4/C_3H_6 mixture containing 1% C_3H_4 (298 K, 1.01 bar) in an absorber bed packed with ELM-12. (b) C_3H_4/C_3H_6 (1/99) separation cycles lasting for 4000 min. Each separation process was carried out at 298 K and 1.01 bar, while regeneration was performed using a He flow (100 mL/min) at 323 K for 30 min.

In summary, we have realized a flexible−robust porous MOF for the challenging task of C_3H_4/C_3H_6 separation/purification. The basic mechanism of this MOF for the specific recognition of C_3H_4 has been clearly demonstrated through neutron diffraction studies and theoretical calculations. The robust guest-free ELM-12 has suitable pore structure as well as strong binding sites to trap C_3H_4 molecules, similar to those revealed in robust MOFs for their recognition of small gas molecules. This work will initiate extensive interest in flexible−robust MOFs for their gas separation and purification properties and thus expand the dictionary of porous MOFs for these very important applications. The high efficiency of ELM-12 to remove the trace C_3H_4 from important raw C_3H_4/C_3H_6 mixtures under ambient conditions to produce high-purity C_3H_6 indicates that this MOF might be potentially useful for this industrially important separation. The realization of this unique porous MOF for the challenging C_3H_4/C_3H_6 separation has initiated the promise of porous MOFs for this very important industrial application. It is expected that extensive research on porous MOFs will eventually lead to some practically useful materials at a reasonable cost in the near future for important hydrocarbon separation and purification processes.

■ ASSOCIATED CONTENT

Supporting Information

The Supporting Information is available free of charge on the ACS Publications website at DOI: 10.1021/jacs.7b04268.

DOI: 10.1021/jacs.7b04268
J. Am. Chem. Soc. 2017, 139, 7733−7736

Experimental procedures, PXRD patterns of ELM-12, crystallographic and refinement parameters for C_3D_4-loaded ELM-12, NPD data, heats of adsorption, adsorption selectivities of C_3H_4/C_3H_6 (1/99 and 50/50) predicted by IAST at 298 K, and regenerability and structural stability data for ELM-12 (PDF)
Crystallographic data for C_3D_4-loaded ELM-12 (CIF)

AUTHOR INFORMATION

Corresponding Authors

*jpli211@hotmail.com
*wzhou@nist.gov
*banglin.chen@utsa.edu

ORCID

Rui-Biao Lin: 0000-0003-3267-220X
Rajamani Krishna: 0000-0002-4784-8530
Bin Li: 0000-0002-7774-5452
Hui Wu: 0000-0003-0296-5204
Jinping Li: 0000-0002-2628-0376
Wei Zhou: 0000-0002-5461-3617
Banglin Chen: 0000-0001-8707-8115

Author Contributions

#L.L. and R.-B.L. contributed equally.

Notes

The authors declare no competing financial interest.

ACKNOWLEDGMENTS

We gratefully acknowledge the financial support from the National Natural Science Foundation of China (21606163), the Natural Science Foundation of Shanxi (201601D021042), and the Welch Foundation (AX-1730).

REFERENCES

(1) (a) Furukawa, H.; Cordova, K. E.; O'Keeffe, M.; Yaghi, O. M. *Science* **2013**, *341*, 1230444. (b) Kitagawa, S.; Kitaura, R.; Noro, S.-i. *Angew. Chem., Int. Ed.* **2004**, *43*, 2334. (c) Wang, C.; Liu, D.; Lin, W. *J. Am. Chem. Soc.* **2013**, *135*, 13222. (d) Chen, B.; Xiang, S.; Qian, G. *Acc. Chem. Res.* **2010**, *43*, 1115. (e) Li, B.; Chrzanowski, M.; Zhang, Y.; Ma, S. *Coord. Chem. Rev.* **2016**, *307*, 106. (f) Yang, S.; Ramirez-Cuesta, A. J.; Newby, R.; Garcia-Sakai, V.; Manuel, P.; Callear, S. K.; Campbell, S. I.; Tang, C. C.; Schröder, M. *Nat. Chem.* **2015**, *7*, 121. (g) Bai, Y.; Dou, Y.; Xie, L.-H.; Rutledge, W.; Li, J.-R.; Zhou, H.-C. *Chem. Soc. Rev.* **2016**, *45*, 2327. (h) Zhu, Q.-L.; Xu, Q. *Chem. Soc. Rev.* **2014**, *43*, 5468. (i) Zhai, Q.-G.; Bu, X.; Mao, C.; Zhao, X.; Daemen, L.; Cheng, Y.; Ramirez-Cuesta, A. J.; Feng, P. *Nat. Commun.* **2016**, *7*, 13645. (j) Cui, Y.; Li, B.; He, H.; Zhou, W.; Chen, B.; Qian, G. *Acc. Chem. Res.* **2016**, *49*, 483. (k) Bao, Z.; Chang, G.; Xing, H.; Krishna, R.; Ren, Q.; Chen, B. *Energy Environ. Sci.* **2016**, *9*, 3612. (l) Howarth, A. J.; Katz, M. J.; Wang, T. C.; Platero-Prats, A. E.; Chapman, K. W.; Hupp, J. T.; Farha, O. K. *J. Am. Chem. Soc.* **2015**, *137*, 7488.

(2) (a) Cui, X.; Chen, K.; Xing, H.; Yang, Q.; Krishna, R.; Bao, Z.; Wu, H.; Zhou, W.; Dong, X.; Han, Y.; Li, B.; Ren, Q.; Zaworotko, M. J.; Chen, B. *Science* **2016**, *353*, 141. (b) Cadiau, A.; Adil, K.; Bhatt, P. M.; Belmabkhout, Y.; Eddaoudi, M. *Science* **2016**, *353*, 137. (c) Nugent, P.; Belmabkhout, Y.; Burd, S. D.; Cairns, A. J.; Luebke, R.; Forrest, K.; Pham, T.; Ma, S.; Space, B.; Wojtas, L.; Eddaoudi, M.; Zaworotko, M. J. *Nature* **2013**, *495*, 80. (d) Bloch, E. D.; Queen, W. L.; Krishna, R.; Zadrozny, J. M.; Brown, C. M.; Long, J. R. *Science* **2012**, *335*, 1606. (e) Hu, T.-L.; Wang, H.; Li, B.; Krishna, R.; Wu, H.; Zhou, W.; Zhao, Y.; Han, Y.; Wang, X.; Zhu, W.; Yao, Z.; Xiang, S.; Chen, B. *Nat. Commun.* **2015**, *6*, 7328. (f) Wang, H.; Yao, K.; Zhang, Z.; Jagiello, J.; Gong, Q.; Han, Y.; Li, J. *Chem. Sci.* **2014**, *5*, 620. (g) Luo, F.; Yan, C.; Dang, L.; Krishna, R.; Zhou, W.; Wu, H.; Dong, X.; Han, Y.; Hu, T.-L.; O'Keeffe, M.; Wang, L.; Luo, M.; Lin, R.-B.; Chen, B. *J. Am. Chem. Soc.* **2016**, *138*, 5678.

(3) (a) Foo, M. L.; Matsuda, R.; Hijikata, Y.; Krishna, R.; Sato, H.; Horike, S.; Hori, A.; Duan, J.; Sato, Y.; Kubota, Y.; Takata, M.; Kitagawa, S. *J. Am. Chem. Soc.* **2016**, *138*, 3022. (b) Horike, S.; Inubushi, Y.; Hori, T.; Fukushima, T.; Kitagawa, S. *Chem. Sci.* **2012**, *3*, 116. (c) Hamon, L.; Llewellyn, P. L.; Devic, T.; Ghoufi, A.; Clet, G.; Guillerm, V.; Pirngruber, G. D.; Maurin, G.; Serre, C.; Driver, G.; van Beek, W.; Jolimaître, E.; Vimont, A.; Daturi, M.; Férey, G. *J. Am. Chem. Soc.* **2009**, *131*, 17490. (d) Lin, R.-B.; Li, L.; Wu, H.; Arman, H.; Li, B.; Lin, R.-G.; Zhou, W.; Chen, B. *J. Am. Chem. Soc.* **2017**, DOI: 10.1021/jacs.7b03850.

(4) Coudert, F.-X.; Mellot-Draznieks, C.; Fuchs, A. H.; Boutin, A. *J. Am. Chem. Soc.* **2009**, *131*, 11329.

(5) (a) Gücüyener, C.; van den Bergh, J.; Gascon, J.; Kapteijn, F. *J. Am. Chem. Soc.* **2010**, *132*, 17704. (b) Liao, P.-Q.; Zhang, W.-X.; Zhang, J.-P.; Chen, X.-M. *Nat. Commun.* **2015**, *6*, 8697.

(6) (a) Grunker, R.; Senkovska, I.; Biedermann, R.; Klein, N.; Lohe, M. R.; Muller, P.; Kaskel, S. *Chem. Commun.* **2011**, *47*, 490. (b) Lin, J.-M.; He, C.-T.; Liao, P.-Q.; Lin, R.-B.; Zhang, J.-P. *Sci. Rep.* **2015**, *5*, 11537. (c) Reichenbach, C.; Kalies, G.; Lincke, J.; Lässig, D.; Krautscheid, H.; Moellmer, J.; Thommes, M. *Microporous Mesoporous Mater.* **2011**, *142*, 592. (d) Kondo, A.; Chinen, A.; Kajiro, H.; Nakagawa, T.; Kato, K.; Takata, M.; Hattori, Y.; Okino, F.; Ohba, T.; Kaneko, K.; Kanoh, H. *Chem. - Eur. J.* **2009**, *15*, 7549.

(7) (a) Kondo, A.; Kajiro, H.; Noguchi, H.; Carlucci, L.; Proserpio, D. M.; Ciani, G.; Kato, K.; Takata, M.; Seki, H.; Sakamoto, M.; Hattori, Y.; Okino, F.; Maeda, K.; Ohba, T.; Kaneko, K.; Kanoh, H. *J. Am. Chem. Soc.* **2011**, *133*, 10512. (b) Kondo, A.; Noguchi, H.; Carlucci, L.; Proserpio, D. M.; Ciani, G.; Kajiro, H.; Ohba, T.; Kanoh, H.; Kaneko, K. *J. Am. Chem. Soc.* **2007**, *129*, 12362.

(8) (a) Friedrich, M. F.; Lucas, M.; Claus, P. *Catal. Commun.* **2017**, *88*, 73. (b) Li, L.; Krishna, R.; Wang, Y.; Yang, J.; Wang, X.; Li, J. *J. Mater. Chem. A* **2016**, *4*, 751. (c) McCue, A. J.; Guerrero-Ruiz, A.; Rodríguez-Ramos, I.; Anderson, J. A. *J. Catal.* **2016**, *340*, 10.

(9) (a) Li, J.-R.; Kuppler, R. J.; Zhou, H.-C. *Chem. Soc. Rev.* **2009**, *38*, 1477. (b) Burghardt, A. In *Chemical Engineering and Chemical Process Technology*; Pohorecki, R., Bridgwater, J., Molzahn, M., Gani, R., Gallegos, C., Eds.; Eolss Publishers Co. Ltd.: Oxford, U.K., 2010; Vol. *1*, p 188.

(10) Kim, Y. J.; Lee, H. J.; Ahn, Y.; Zhang, S.; Lee, J. S.; Cheong, M.; Kim, H. S. *Phys. Chem. Chem. Phys.* **2017**, *19*, 2168.

DOI: 10.1021/jacs.7b04268
J. Am. Chem. Soc. 2017, 139, 7733−7736

Supporting Information

Flexible-Robust Metal-Organic Framework for Efficient Removal of Propyne from Propylene

Libo Li,[a,b,e,#] Rui-Biao Lin,[b,#] Rajamani Krishna,[c] Xiaoqing Wang,[a,e] Bin Li,[b] Hui Wu,[d] Jinping Li,[a,e,*] Wei Zhou,[d,*] and Banglin Chen[b,*]

[a]College of Chemistry and Chemical Engineering, Taiyuan University of Technology, Taiyuan 030024, Shanxi, P. R. China

[b]Department of Chemistry, University of Texas at San Antonio, One UTSA Circle, San Antonio, TX 78249-0698, United States

[c]Van 't Hoff Institute for Molecular Sciences, University of Amsterdam, Science Park 904, 1098 XH Amsterdam, The Netherlands

[d]NIST Center for Neutron Research, National Institute of Standards and Technology, Gaithersburg, MD 20899-6102, United States

[e]Shanxi Key Laboratory of Gas Energy Efficient and Clean Utilization, Taiyuan 030024, Shanxi, P. R. China

Table of Contents

1. Experimental section

1.1 Materials

$[Cu(bpy)_2(OTf)_2]$ (ELM-12): The synthetic method described by Kondo et al.[1] was improved as follows: A solution of bpy (10.0 mmol/L, 10.0 mL) in ethanol was carefully layered onto an aqueous solution (10 mL) of $Cu(OTf)_2$ (5 mmol/L) in a watch glass with no stirring. Then, the mixture was placed in a 298 K in cubator for 7 days to give sheet crystals as $[Cu(bpy)_2(OTf)_2]\cdot 2EtOH\cdot H_2O$. Then, the crystals were collected and activated under 10^{-6} bar at 393 K until no further weight loss was observed to give $[Cu(bpy)_2(OTf)_2]$ as a guest free struture. $[Cu(bpy)_2(OTf)_2]$ has 2D structure, which was constructed with Cu^{2+} and bpy as the layer and bridging OTf^- to integrated into a three-dimensional structure.

1.2 Powder x-ray diffraction experiment and FTIR spectroscopy

The crystallinities and phase purities of the samples were measured by powder X-ray diffraction (PXRD) with a Rigaku Mini Flex II X-ray diffractometer employing Cu-K_α radiation operated at 30 kV and 15 mA, scanning over the range 5–40° (2θ) at a rate of 1°/min. Fourier Transform infrared (FTIR) spectroscopy was performed by using an IRAffinity-1 (SHIMADZU) spectrometer.

1.3 Neutron diffraction experiment

Powder neutron diffraction data were collected using the BT-1 neutron powder diffractometer at the National Institute of Standards and Technology (NIST) Centre for Neutron Research. A Ge(311) monochromator with a 75° take-off angle, λ = 2.0787(2) Å, and in-pile collimation of 60 minutes of *arc* was used. Data were collected over the range of 1.3-166.3° (2θ) with a step size of 0.05°. Fully activated ELM-12 sample was loaded in a vanadium can equipped with a capillary gas line. A closed-cycle He refrigerator was used to control the sample temperature. The bare MOF sample was measured first at the temperatures of 298 K. To probe the propyne adsorption locations, a pre-determined pressure (1 bar) of C_3D_4 was loaded into the sample at room temperature. Diffraction data were then collected on the C_3D_4-loaded MOF sample. Rietveld structural refinement was performed on the neutron diffraction data using the GSAS package.[2] Refinement on lattice parameters, atomic coordinates, thermal factors, gas molecule occupancies, background, and profiles all converge with satisfactory R-factors. Crystallographic data and refinement information are summarized in Table S1. CCDC 1545782 contains the supplementary crystallographic data of C_3D_4-loaded ELM-12. This data can be obtained free of charge from the Cambridge Crystallographic Data Centre via www.ccdc.cam.ac.uk/data_request/cif.

1.4 Density-functional theory calculations

Density-functional theory (DFT) calculations were performed using the Quantum-Espresso package.[3] A semi-empirical addition of dispersive forces to conventional DFT was included in the calculation to account for van der Waals

interactions.[4] We first optimized the structure of ELM-12, the optimized structure agrees well with the reported ELM-12 (Guest-free) structure.[1] C_3H_4 and C_3H_6 guest gas molecules were then introduced to various locations of the MOF pore, followed by a full structural relaxation. The static binding energy (at T = 0 K) was calculated using: E_B = E(MOF) + E(gas) – E(MOF+gas).

1.5 Single-component adsorption measurements

The purities of the propyne and propylene are higher than 99.9999%. Their adsorption isotherms were collected with an Intelligent Gravimetric Analyser (IGA 001, Hiden, UK). Samples were activated overnight under vacuum at 393 K or until no further weight loss was observed.

1.6 Breakthrough separation experiments

The breakthrough curves of were measured on a homemade apparatus for gases mixtures C_3H_4/C_3H_6 (1/99) and C_3H_4/C_3H_6 (50/50) at 298 K and 1.01 bar. In the separation experiment, ELM-12 (4.1380 g) particles with diameters of 200-300 μm were prepared and packed into Φ 9×150 mm stainless steel column, and the column was activated under reduced pressure at 393 K overnight. The experimental set-up consisted of two fixed-bed stainless steel reactors. One reactor was loaded with the adsorbent, while the other reactor was used as a blank control group to stabilize the gas flow. The gas flows were controlled at the inlet by a mass flow meter as 2 mL/min, and a gas chromatograph (TCD-Thermal Conductivity Detector, detection limit 0.1 ppm) continuously monitored the effluent gas from the adsorption bed. Prior to every breakthrough experiment, we activated the sample by flushing the adsorption bed with helium gas for 2 hours at 373 K. Subsequently, the column was allowed to equilibrate at the measurement rate before we switched the gas flow.

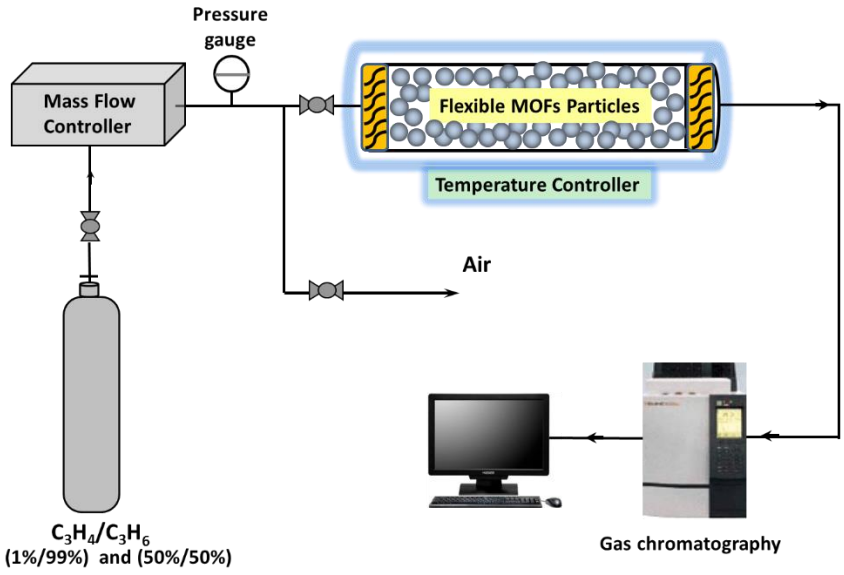

Breakthrough experiments apparatus

2. Calculation of the separation potential of ELM-12

2.1 Fitting of pure component isotherms

The experimentally measured excess loadings for C_3H_4 and C_3H_6 at temperatures of 273 and 298 K for ELM-12 were fitted with the dual-Langmuir-Freundlich isotherm model

$$q = q_{A,sat}\frac{b_A p^{\nu_A}}{1+b_A p^{\nu_A}} + q_{B,sat}\frac{b_B p^{\nu_B}}{1+b_B p^{\nu_B}}$$

with T-dependent parameters b_A, and b_B

$$b_A = b_{A0}\exp\left(\frac{E_A}{RT}\right); \quad b_B = b_{B0}\exp\left(\frac{E_B}{RT}\right)$$

The parameters are provided in Table S3.

2.2 Isosteric heat of adsorption

The binding energies of C_3H_4, and C_3H_6 for ELM-12 are reflected in the isosteric heat of adsorption (Figure S2), Q_{st}, defined as

$$Q_{st} = RT^2\left(\frac{\partial \ln p}{\partial T}\right)_q$$

These values were determined by analytic differentiation of the pure component isotherm fits.

2.3 IAST calculations of adsorption selectivities

In order to establish the feasibility of C_3H_4/C_3H_6 separations we performed calculations using the ideal adsorbed solution theory (IAST) of Myers and Prausnitz.[5] The adsorption selectivities and uptakes were determined for 1/99 (Figure 1e) and 50/50 C_3H_4/C_3H_6 (Figure S3) mixtures at 298 K.

2.4 Transient breakthrough simulations

The performance of industrial fixed bed adsorbers is dictated by a combination of adsorption selectivity and uptake capacity. For a proper comparison of various MOFs, we perform transient breakthrough simulations using the simulation methodology described in the literature (Figure S8).[6] For the breakthrough simulations, the following parameter values were used: length of packed bed, L = 0.3 m; voidage of packed bed, ε = 0.4; superficial gas velocity at inlet, u = 0.04 m/s. The framework density of ELM-12 is 1406 kg m^{-3}. The transient breakthrough simulation results are presented in terms of a *dimensionless* time, τ, defined by dividing the actual time, t, by the characteristic time, $\frac{L\varepsilon}{u}$.

Notation

b_A	Langmuir-Freundlich constant for species *i* at adsorption site A, $Pa^{-\nu_{iA}}$
b_B	Langmuir-Freundlich constant for species *i* at adsorption site B, $Pa^{-\nu_{iB}}$
c_i	molar concentration of species *i* in gas mixture, mol m^{-3}
c_{i0}	molar concentration of species *i* in gas mixture at inlet to adsorber, mol m^{-3}
E	energy parameter, J mol^{-1}
L	length of packed bed adsorber, m
p_i	partial pressure of species *i* in mixture, Pa
p_t	total system pressure, Pa
q_i	component molar loading of species *i*, mol kg^{-1}
Q_{st}	isosteric heat of adsorption, J mol^{-1}
t	time, s
T	absolute temperature, K
u	superficial gas velocity in packed bed, m s^{-1}

Greek letters

ε	voidage of packed bed, dimensionless
ν	Freundlich exponent, dimensionless
ρ	framework density, kg m^{-3}
τ	time, dimensionless

References

[1] Kondo, A.; Noguchi, H.; Carlucci, L.; Proserpio, D. M.; Ciani, G.; Kajiro, H.; Ohba, T.; Kanoh, H.; Kaneko, K. *J. Am. Chem. Soc.* **2007**, *129*, 12362.

[2] Larson, A. C.; Von Dreele, R. B. General Structure Analysis System, Report LAUR 86-748; Los Alamos National Laboratory: Los Alamos, NM, **1994**.

[3] Giannozzi, P.; Baroni, S.; Bonini, N.; Calandra, M.; Car, R.; Cavazzoni, C.; Ceresoli, D.; Chiarotti, G. L.; Cococcioni, M.; Dabo, I.; Dal Corso, A.; de Gironcoli, S.; Fabris, S.; Fratesi, G.; Gebauer, R.; Gerstmann, U.; Gougoussis, C.; Kokalj, A.; Lazzeri, M.; Martin-Samos, L.; Marzari, N.; Mauri, F.; Mazzarello, R.; Paolini, S.; Pasquarello, A.; Paulatto, L.; Sbraccia, C.; Scandolo, S.; Sclauzero, G.; Seitsonen, A. P.; Smogunov, A.; Umari, P.; Wentzcovitch, R. M. *J. Phys.: Condens. Matter* **2009**, *21*, 395502.

[4] Barone, V.; Casarin, M.; Forrer, D.; Pavone, M.; Sambi, M.; Vittadini, A. *J. Comput. Chem.* **2009**, *30*, 934.

[5] Myers, A. L.; Prausnitz, J. M. *A.I.Ch.E.J.* **1965**, 11, 121.

[6] Krishna, R. *RSC Adv.* **2015**, 5, 52269.

3. Synthesis and characterization of ELM-12.

3.1 Crystal structure of ELM-12.

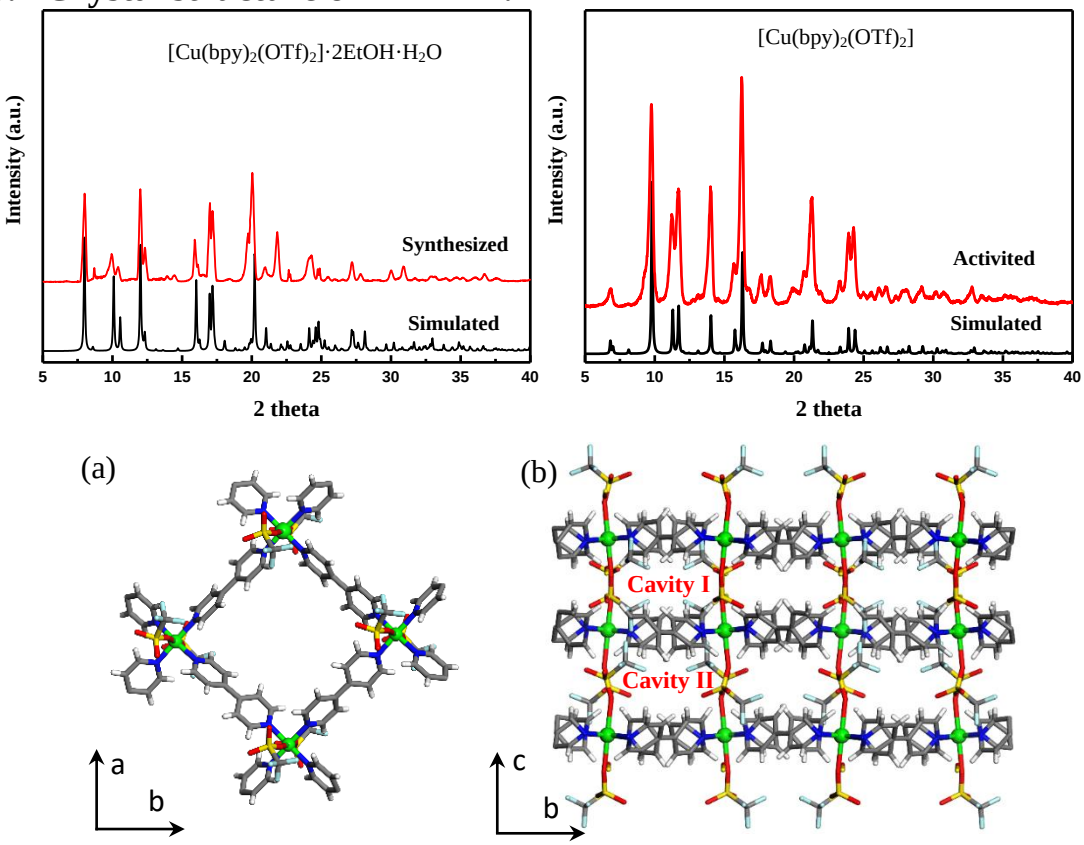

Figure S1. Powder X-ray diffraction (PXRD) patterns of the synthesized and activated ELM-12 samples are very similar to simulated structural data, which further confirm the phase purity of these samples. (a-b) ELM-12 consists of a rigid square-grid copper bipyridine scaffold with dynamic dangling OTf^- groups. After the guest removal, ELM-12 still shows porosity with two kinds of cavities (cavity I and II) (Cu, green; C, gray; O, red; H, white; S, yellow; F, blue).

Calculation of the separation potential of ELM-12

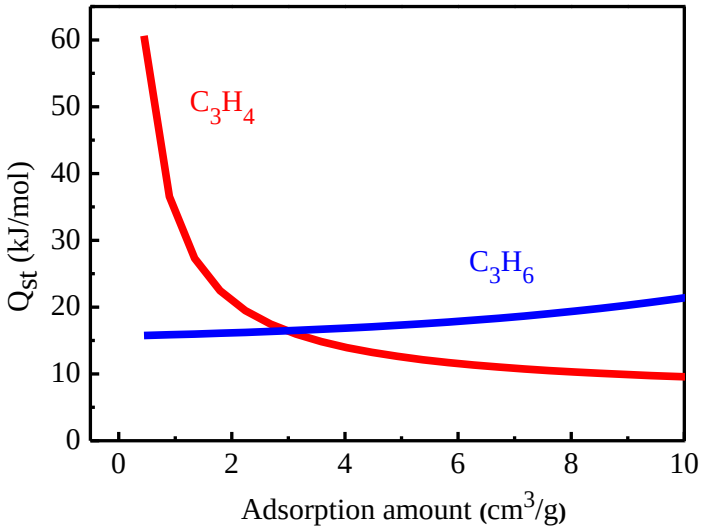

Figure S2. Adsorption heat of C_3H_4 (red) and C_3H_6 (blue) for ELM-12, respectively.

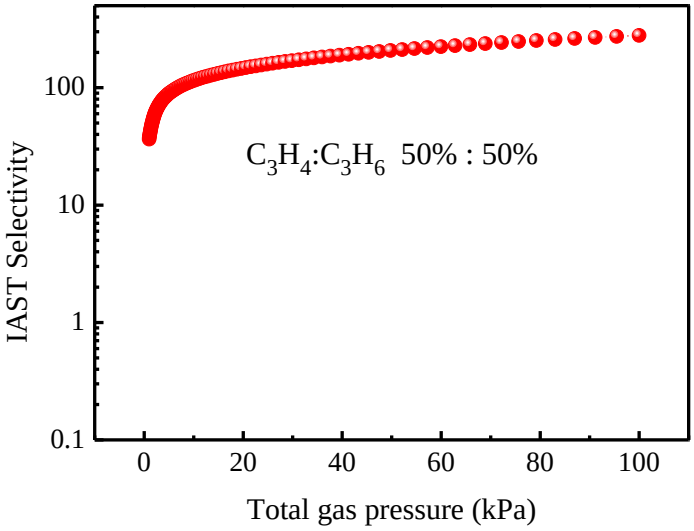

Figure S3. IAST selectivity of ELM-12 for C_3H_4/C_3H_6 (50/50) mixtures at 298 K.

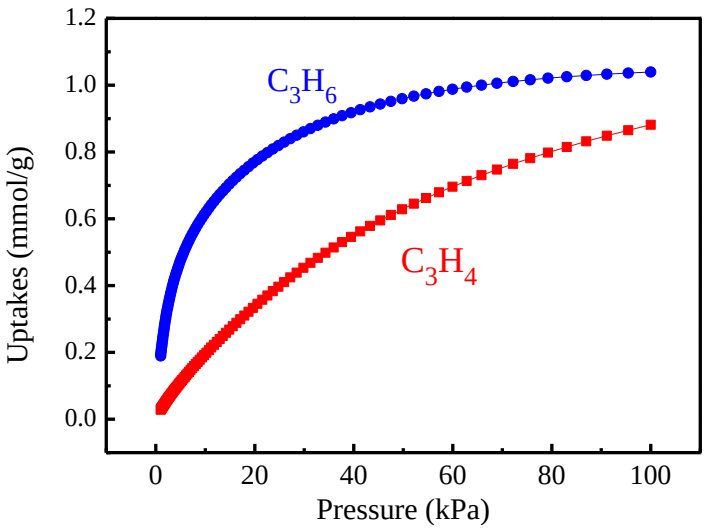

Figure S4. Mixture adsorption isotherms predicted by IAST of ELM-12 for C_3H_4/C_3H_6 (1/99) mixtures at 298 K.

3.2 Crystallographic data of C_3D_4-loaded ELM-12

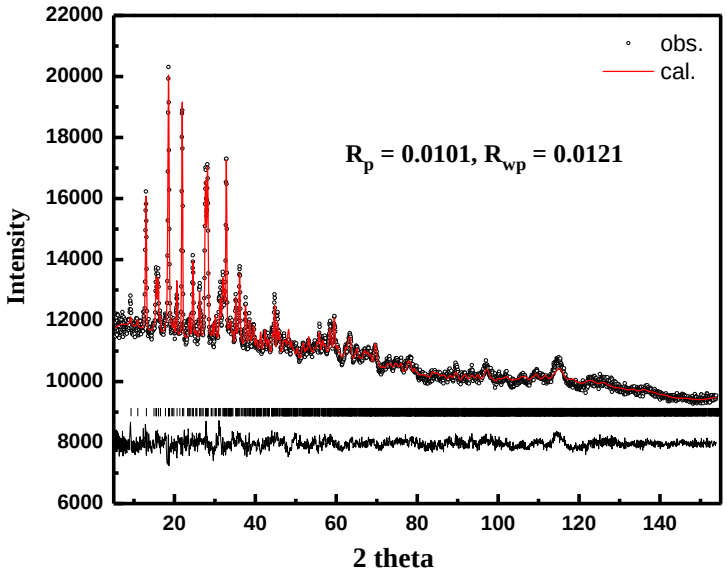

Figure S5. Experimental (circles), calculated (line), and difference (line below observed and calculated patterns) powder neutron diffraction profiles for a C_3D_4-loaded sample of ELM-12 measured at 298 K. Goodness of fit parameters of the Rietveld refinement are shown as insets.

Structural comparison of guest-free and C_3D_4-loaded ELM-12

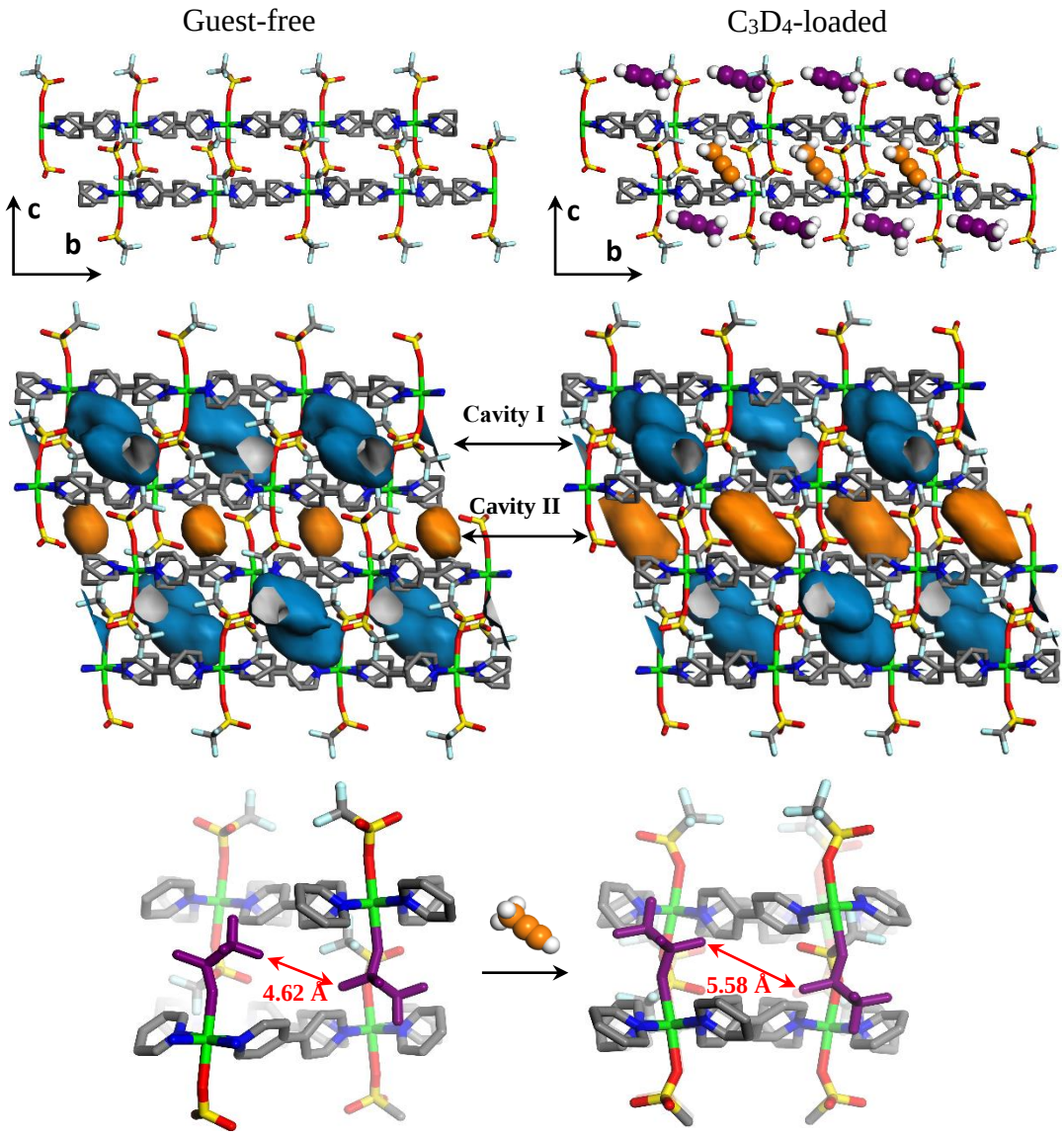

Figure S6. The two preferential C_3D_4 binding sites and structure-change of ELM-12, as determined by neutron powder diffraction. Cavity II has slightly expansion from 6.8 × 4.0 × 4.2 $Å^3$ to 7.2 × 4.2 × 4.3 $Å^3$ after the C_3D_4 adsorption, which indicates the relatively strong host-guest interaction between C_3D_4 and ELM-12.

4. C_3H_6 adsorption in ELM-12 calculated by DFT-D method.

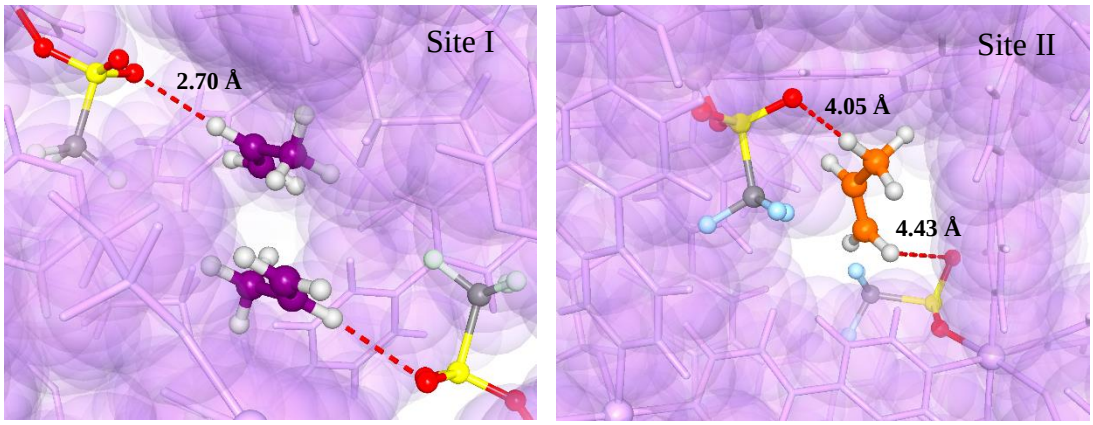

Figure S7. First-principles DFT-D-calculated C_3H_6 binding sites (the nearest H···O distance: site I ~2.70 Å; site II ~4.05–4.43 Å) in ELM-12. The calculated static binding energies are ~32.3 (site I) and 25.6 kJ/mol (site II) for the two adsorption sites, respectively.

Dynamic adsorption on ELM-12

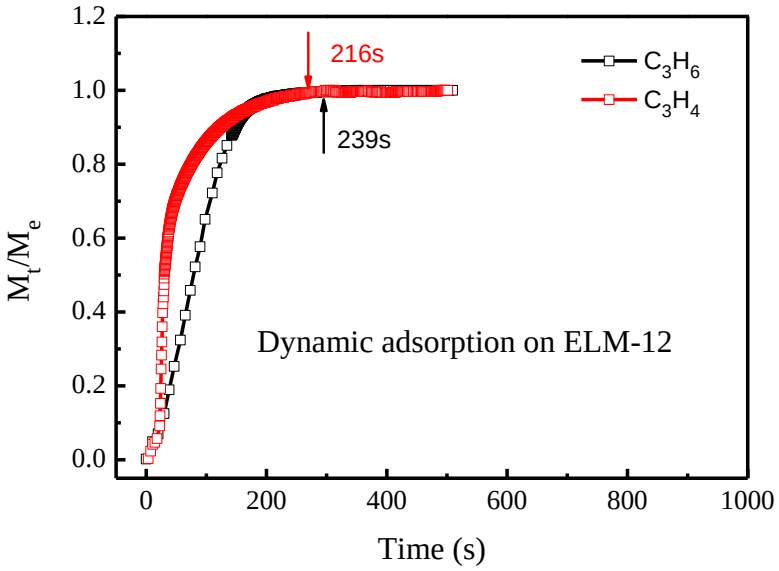

Figure S8. C_3H_4 and C_3H_6 dynamic adsorption on ELM-12 at 298 K and 1 bar. The results showed that C_3H_4 and C_3H_6 have the similar adsorption equilibrium time, the difference of diffusion rates of C_3H_4 and C_3H_6 is negligible. Therefore, high C_3H_4/C_3H_6 selectivity can be mainly attributed to the binding and sieving effect of ELM-12.

5. Breakthrough curves for C_3H_4/C_3H_6 separation

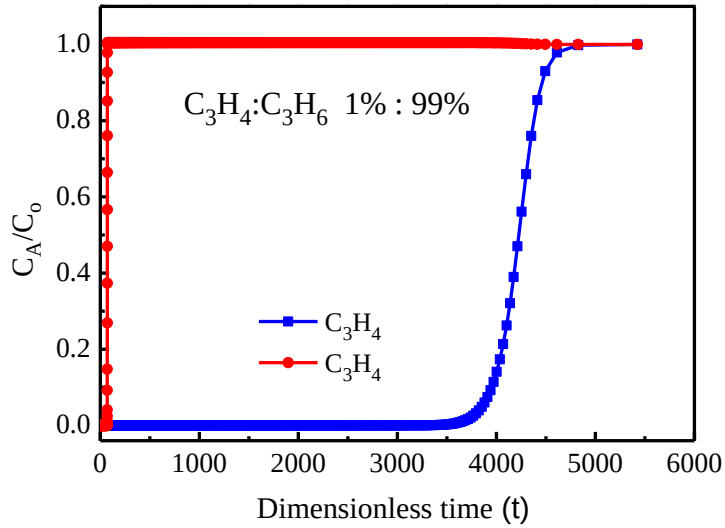

Figure S9. Simulated column breakthrough curves for C_3H_4/C_3H_6 (1/99) mixtures separation.

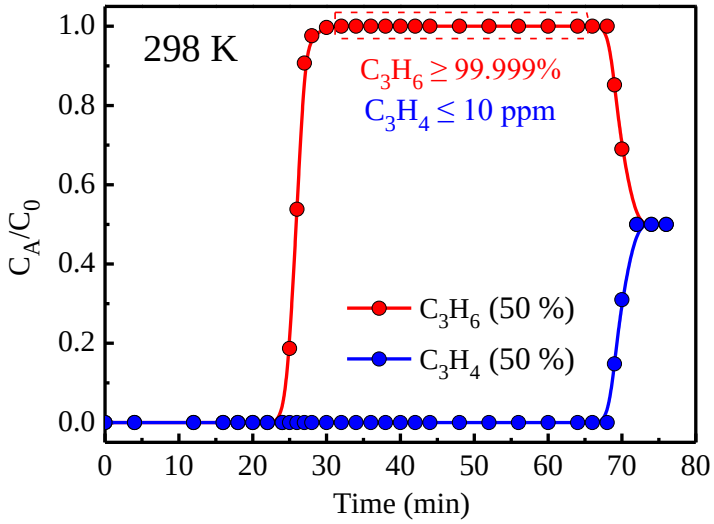

Figure S10. Experimental breakthrough curves of C_3H_4/C_3H_6 (50/50) mixtures separation for ELM-12 materials at 298 K and 1.01 bar.

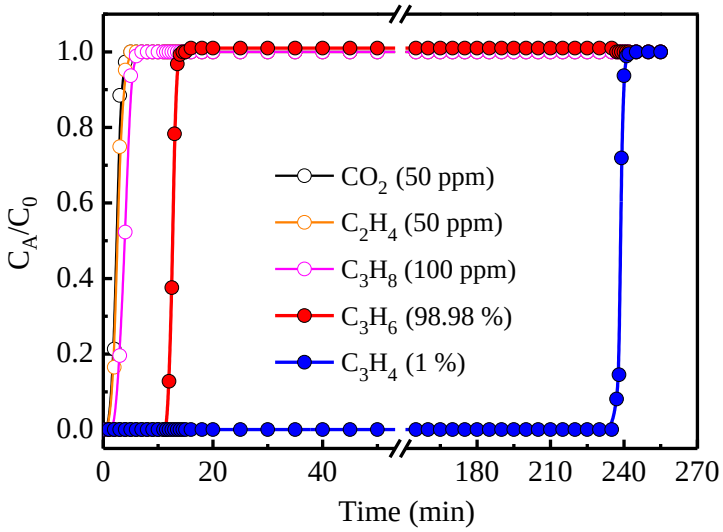

Figure S11. Experimental breakthrough curves for separation of (1/98.98/0.01/0.005/0.005) $C_3H_4/C_3H_6/C_3H_8/C_2H_4/CO_2$ mixtures at 298 K and 1.01 bar.

6. **Adsorption cycling experiments for ELM-12**

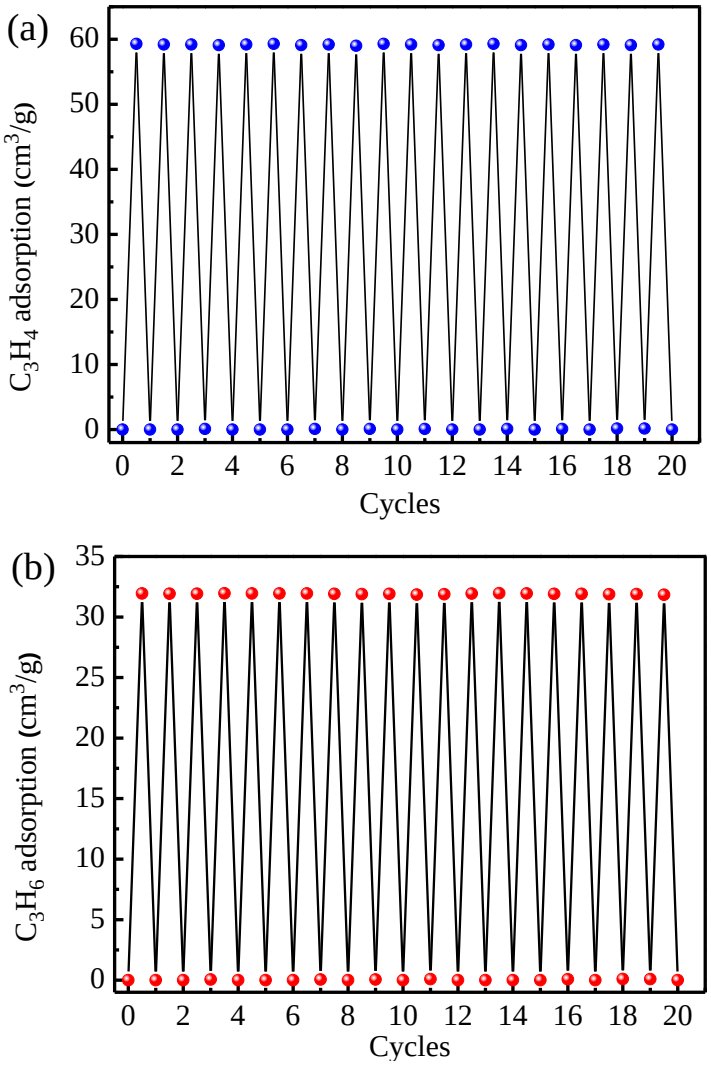

Figure S12. C_3H_4 (a) and C_3H_6 (b) adsorption cycles for ELM-12. After each adsorption process, sample was evacuated under 10^{-6} bar for 30 minutes.

7. **Separation cycling experiments for ELM-12**

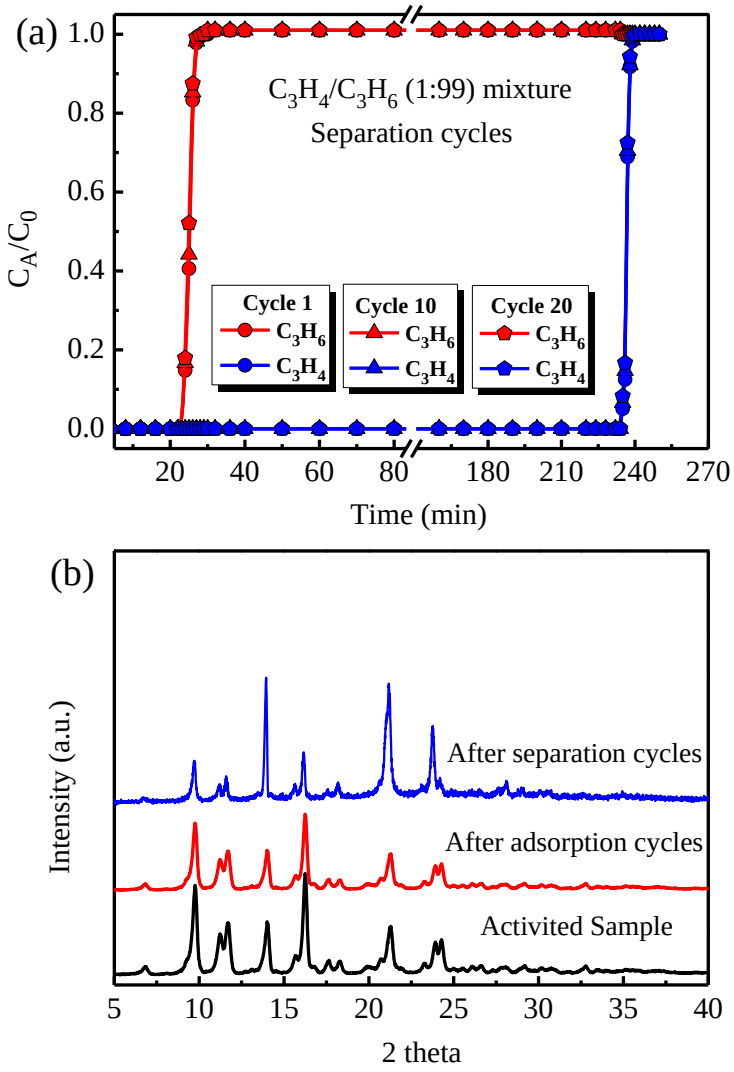

Figure S13. (a) Cycling column breakthrough curves of C_3H_4/C_3H_6 separation (1/99) for ELM-12 at 298 K and 1 bar. The breakthrough experiments were carried out at a flow rate of 2 mL/min. Regeneration with He flow (100 mL/min) for 2 hours at 323 K. (b) PXRD patterns of ELM-12 samples after adsorption and separation cycles.

8. **Structural stability experiments for ELM-12**

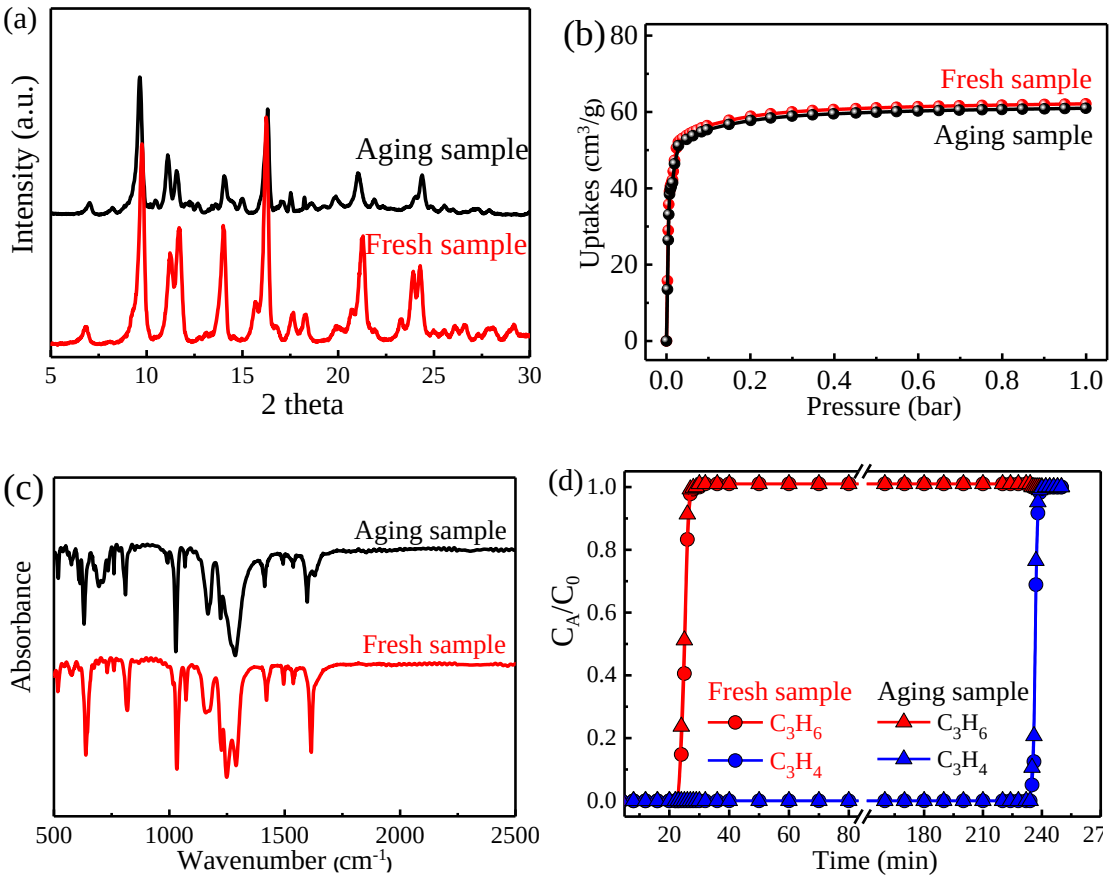

Figure S14. (a) PXRD, (b) C_3H_4 adsorption, (c) FTIR spectroscopy, and (d) breakthrough experiment of C_3H_4/C_3H_6 (1/99) mixture for ELM-12 samples (fresh sample and two-years aging sample), respectively.

Table S1. Comparison of the crystallographic and refinement parameters for guest-free and C_3D_4-loaded ELM-12.

Crystal data	ELM-12 (Guest-free)[#]	ELM-12 (C_3D_4)
System	Monoclinic	Monoclinic
Space group	*C*2/*c*	*C*2/*c*
MF	$C_{22}H_{16}CuF_6N_4O_6S_2$	$C_{24}H_{16}CuD_3F_6N_4O_6S_2$
FW	674.05	706.28
a/Å	27.08	27.499
b/Å	15.096	14.9307
c/Å	16.136	16.565
$\alpha/^o$	90.00	90.0
$\beta/^o$	111.344	110.550
$\gamma/^o$	90.00	90.0
Volume/Å^3	6144	6368.6
Z	8	8
Density/g/cm^3	1.457	1.406
Theoretical pore volume/cm^3/g	0.141[a]	0.145[a]
Refinement indices	R_1 = 0. 1415, wR_2 = 0.3556	R_p = 0.0101, R_{wp} = 0.0121

[a] Calculated based on the MOF crystal structures using PLATON software.

[#] Parameters from Kondo, A. et al. *J. Am. Chem. Soc.* **2007**, *129*, 12362.

Table S2. Comparison of porosity parameters for guest-free, C_3D_4-loaded (298 K) and N_2-loaded (77 K) ELM-12.

Crystal data	ELM-12 (Guest-free)[#]	ELM-12 (C_3D_4)	ELM-12 (N_2)[#]
Theoretical pore volume/cm^3/g	0.141	0.145	0.287
Density/g/cm^3	1.457	1.406	1.321
Porosity	20.5%	20.4%	38 %

[#] Kondo, A. et al. *J. Am. Chem. Soc.* **2007**, *129*, 12362.

Table S3. Dual-Langmuir-Freundlich fitting parameters for C_3H_4 and C_3H_6 isotherms.

	Site A				Site B			
	$q_{A,sat}$ mol kg^{-1}	b_{A0} $Pa^{-\nu_i}$	E_A kJ mol^{-1}	ν_A dimensionless	$q_{B,sat}$ mol kg^{-1}	b_{B0} $Pa^{-\nu_i}$	E_B kJ mol^{-1}	ν_B dimensionless
C_3H_4	2.2	2.07×10^{-5}	5	1.45	1.2	4.47×10^{-12}	52	0.45
C_3H_6	1.5	6.62×10^{-12}	36	1	0.6	1.46×10^{-6}	14	1